Title	Observation of enhanced visible and infrared emissions in photonic crystal thin-film light-emitting diodes
Author(s)	Cheung, YF; Li, KH; Hui, RSY; Choi, HW
Citation	Applied Physics Letters , 2014, v. 105 n. 7, article no. 071104, p. 071104:1-4
Issued Date	2014
URL	http://hdl.handle.net/10722/202850
Rights	Applied Physics Letters . Copyright © American Institute of Physics.

Observation of enhanced visible and infrared emissions in photonic crystal thin-film light-emitting diodes

Y. F. Cheung, K. H. Li, R. S. Y. Hui, and H. W. Choi

Citation: Applied Physics Letters **105**, 071104 (2014); doi: 10.1063/1.4893739
View online: http://dx.doi.org/10.1063/1.4893739
View Table of Contents: http://scitation.aip.org/content/aip/journal/apl/105/7?ver=pdfcov
Published by the AIP Publishing

Observation of enhanced visible and infrared emissions in photonic crystal thin-film light-emitting diodes

Y. F. Cheung,[a] K. H. Li,[a] R. S. Y. Hui, and H. W. Choi[b]
Department of Electrical and Electronic Engineering, The University of Hong Kong, Pokfulam Road, Hong Kong

(Received 6 June 2014; accepted 11 August 2014; published online 19 August 2014)

Photonic crystals, in the form of closed-packed nano-pillar arrays patterned by nanosphere lithography, have been formed on the n-faces of InGaN thin-film vertical light-emitting diodes (LEDs). Through laser lift-off of the sapphire substrate, the thin-film LEDs conduct vertically with reduced dynamic resistances, as well as reduced thermal resistances. The photonic crystal plays a role in enhancing light extraction, not only at visible wavelengths but also at infrared wavelengths boosting heat radiation at high currents, so that heat-induced effects on internal quantum efficiencies are minimized. The observations are consistent with predictions from finite-difference time-domain simulations. © *2014 AIP Publishing LLC*. [http://dx.doi.org/10.1063/1.4893739]

Devices based on the III-nitride direct bandgap semiconductor have seamlessly integrated into our daily lives, having been adopted in a wide range of domestic and industrial products, ranging from traffic lamps, indoor/outdoor illumination, and display backlights to panel displays. While such solid-state emitters are generally more energy-efficient than their predecessors, their performances are often limited by heat-related side effects at high-current operations, including brightness recession, color shift and lifetime shortening. The thermal performances of GaN-on-sapphire light-emitting diodes (LEDs) are limited by the poor thermal conductivity of sapphire. Integration with cooling components such as heat-sinks or even peltier coolers improves heat dissipation but makes the manufacturing process more tedious and costly. Optically, light extraction is degraded by trapping of light within sapphire and optical absorption of the current spreading layer, typically indium-tin-oxide (ITO), which is necessitated due to the high resistivities of p-type GaN. The laser lift-off (LLO) technique,[1] being capable of separating the epitaxial GaN film from its sapphire substrate, allows both faces of the semiconductor film to be accessible for contacting, thus enabling vertical conduction. From the electrical conduction point of view, the vertical structure offers optimal current spreading along the high-conductance n-GaN layer to avoid current crowding effects[2] and reduces power consumption due to reduced resistances.

Although electrical and thermal conduction are optimized in vertical LEDs, their optical characteristics are hardly different from laterally conducting LEDs, suffering from limited light extraction due total internal reflections at the high refractive-index-contrast of GaN/air interface, so that the trapped photons would end up being re-absorbed. Different approaches have been introduced to assist with extraction of the laterally guided light, including random surface roughening,[3] chip-shaping,[4,5] micro-pixelation,[6,7] and ordered nanostructuring. In particular, two-dimensional (2-D) photonic crystals (PhCs),[8,9] typically in the form of arrays of air-holes or pillars inscribed on the light-emitting surfaces, have been demonstrated to have the capability of redirecting photons in guided modes into free space. Whilst there have been vast numbers of papers reporting on PhC effects at visible and ultraviolet wavelengths, its role at infrared (IR) wavelengths for InGaN LEDs has not been considered. Understanding the optical properties of the PhC in the IR region is meaningful even though the devices emit in the visible, as the temperatures of the chips are directly affected by IR radiation, a means of heat loss particularly at elevated temperatures. In this study, the optical and thermal effects of a thin-film InGaN LED incorporating 2-D PhC patterned by nanosphere lithography (NSL) are investigated. The thin-film platform is ideal for such studies, as it allows the devices to be driven harder. Apart from the established effects of improved electrical and optical (at visible wavelengths) performances, the PhC is found to enhance extraction of infrared light simultaneously, contributing to improved heat dissipation via radiation at high-power operations.

The wafers used in this study are grown on c-plane sapphire substrates by metal-organic chemical vapor deposition (MOCVD). The epitaxial structure consists of 3 μm of undoped GaN, 2.5 μm of Si-doped GaN, 10 periods of InGaN/GaN quantum wells with center emission wavelength of ~470 nm, and capped with a 0.25 μm Mg-doped contact GaN layer. 200 nm of ITO is deposited on top of p-GaN as a current spreading layer. The sapphire surface is polished to optical smoothness, and the wafer is diced into samples of $5 \times 5\,mm^2$ by laser micro-machining, which are then mounted p-face downwards onto Cu submounts. The collimated beam from a 266-nm Nd:YAG laser (Continuum Surelite) is uniformly irradiated through the sapphire surfaces of the samples for LLO, during which GaN decomposes into gaseous N_2 and Ga droplets at the interface, after which the entire sapphire substrate can be mechanically removed. The detached films are then immersed into dilute HCl for dissolving the residual droplets. To expose the n-GaN contact layer, the undoped GaN layer is removed by inductively coupled plasma (ICP) etching using gaseous mixture of BCl_3 and He, at a pressure

[a]Y. F. Cheung and K. H. Li contributed equally to this work.
[b]Author to whom correspondence should be addressed. Electronic mail: hwchoi@hku.hk. Tel.: (852) 28592693. FAX: (852) 25598738.

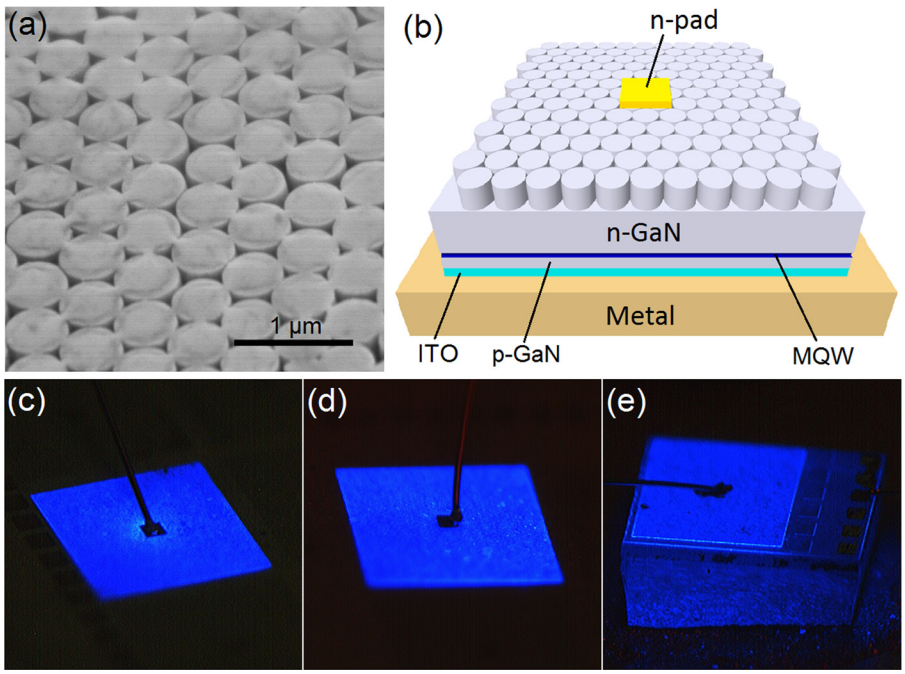

FIG. 1. (a) FE-SEM image showing the HCP nano-pillar array fabricated by NSL. (b) Schematic diagram (not-to-scale) of the vertical PhC thin-film LED. Microphotographs of the (c) V-PhCLED, (d) V-LED, and (e) L-LED.

of 5 mTorr with platen and coil RF powers of 100 W and 400 W, respectively. A monolayer of hexagonally-closed-packed (HCP) silica nanospheres with nominal diameters of 500 nm is spin-coated onto the exposed n-GaN surface; details of the coating process can be found in Ref. 10. The coated samples are then subjected to ICP etching for pattern transfer. After removal of spheres through sonification, a nano-pillar array with diameter of 500 nm and height of 600 nm is formed, as shown in the scanning electron microscope (SEM) image of Fig. 1(a). The device mesa is then photo-lithographically defined so that the unmasked regions are etched by ICP. After a second photo-lithographic definition, Ti/Al/Ti/Au electrodes are deposited by e-beam evaporation, subsequently annealed in nitrogen ambient to form ohmic contacts. The schematic diagram of a vertical PhC thin-film LED (denoted V-PhCLED thereafter) is depicted in Fig. 1(b). For comparison, a thin-film LED without PhC (V-LED) and a conventional laterally conducting GaN-on-sapphire LED (L-LED) are also fabricated. All three devices, with identical mesa areas of $600 \times 600\ \mu m^2$, are wire-bonded but unencapsulated for evaluation. Microphotographs of the three emitting devices are shown in Figs. 1(c)–1(e).

The light output intensity-current-voltage (L-I-V) characteristics of the packaged devices are plotted in Fig. 2. At an injection current of 20 mA, the forward voltages of the L-LED, V-LED, and V-PhCLED as extracted from the plot are 4.0 V, 3.0 V, and 3.2 V, respectively. Expectedly, the vertical configuration allows higher currents to flow through the equally sized junctions at the same bias voltage, due to significant shortening of the current conduction pathway from hundreds of microns in a laterally conducting LED to microns, thereby reducing resistances. Likewise, the dynamic resistances of the V-LED and V-PhCLED of 8.1 Ω and 7.7 Ω, respectively, as determined from the slopes of the I-V curves in the linear regions, are significantly lower than that of the L-LED of 43.8 Ω. Notably, formation of the PhC on the n-face has no adverse effects on the electrical characteristics despite involving plasma processes;[11] the same would not have been true for p-GaN patterning.

Electroluminescence (EL) measurements are conducted to characterize the optical performance of the LEDs. The light emitted from the packaged devices is collected within a 4-in. integrating sphere coupled to a radiometrically calibrated spectrometer via an optical fiber. At lower currents, the optical power of the L-LED rises almost linearly with increasing currents, as shown in the L-I curves of Fig. 2, before thermal effects set in. With further increases of currents, the rate of increase of output power declines and the optical output eventually saturates at currents above 120 mA. For the thin-film devices, the L-I relations remain nearly linear over the measured current range, having been spared of heat-induced degradations. At 20 mA, the V-LED and V-PhCLED emit ~28% and ~42% more light than the L-LED, respectively. The 28% enhancement of the V-LED over the L-LED can be attributed to a combination of reduced absorption due to the removal of the light-absorbing sapphire, as well as direct extraction of light from GaN to air without

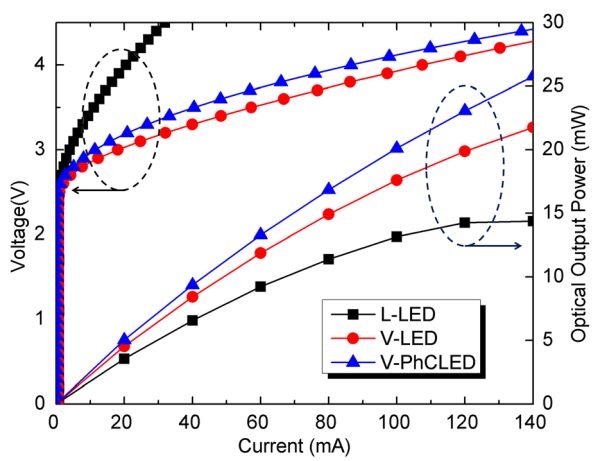

FIG. 2. Plots of L-I-V characteristics of the packaged devices.

having to pass through the light-absorbing ITO layer. Thermal effects are assumed to be negligible at this low current. The additional 14% offered by the V-PhCLED over the V-LED is a result of "weak" photonic crystal effects on light extraction. Note that the closed-packed nano-pillar array does not possess a photonic bandgap; instead, it causes band folding at the Brillouin zone edge so that light from guided modes is coupled into leaky modes above the light line[12] thus promoting light extraction. The band folding capability of PhC is evident from the computed transverse electric (TE) band structure, as shown in Fig. 3(a) (TE mode dominates emissions from InGaN/GaN MQWs (Ref. 13)). A finite-difference time-domain (FDTD) simulation is also conducted to study the interaction of light with the PhC, based on 3-D models constructed according to the fabricated structure, injected with a continuous-wave dipole at $\lambda = 470$ nm (being λ_{peak} of the LEDs). The simulated plots of electric-field intensity distribution for an unpatterned GaN/air interface and the PhC are illustrated in Figs. 3(b) and 3(c), respectively. Quantitatively, the simulation predicts that the PhC increases light transmission by ~11.2% compared with a flat interface, consistent with experimental results.

At higher currents, light extraction effects remain unchanged, while thermal effects begin to kick in. In the L-LED, the reducing rate of increase of output power is mainly due to the drop of internal quantum efficiencies (IQE) at elevated temperatures. At a current of 140 mA, the V-LED emits 51% more optical power than the L-LED, of which 28% had been attributed to temperature-independent light extraction effects. The thermal effect on the L-LED is associated with the sapphire substrate with high thermal resistance. One would then expect thermal effects to be identical in both vertical LEDs with identical thermal conduction pathways, but this is found not to be the case. As observed from Fig. 2, the L-I characteristics of the V-LED appear to deviate from linearity at high currents to a greater extent than the V-PhCLED. For a clearer view, the light output enhancement ratios of the V-PhCLED over the V-LED at different currents are plotted in Fig. 4(a); the ratio increases from 11% to 18% as the current is raised from 20 to 140 mA. Noting that light extraction is temperature independent, the observation suggests that the temperature of V-LED is higher than that of the V-PhCLED.

The surface temperatures of the LEDs are measured by infrared thermometry using a long-wave infrared (LWIR) camera (FLIR SC645) adopting emissivity values for GaN and ITO of 0.62 and 0.265, respectively, which have been experimentally determined by comparison with a reference heat source. Multiple data points are taken across the LEDs from the LWIR map, from which an average temperature is evaluated and the standard error of measurement is 0.89%. Figure 4(b) plots the average surface temperatures of the three devices as functions of currents. At 20 mA, the measured temperatures of all LEDs are nearly identical and are

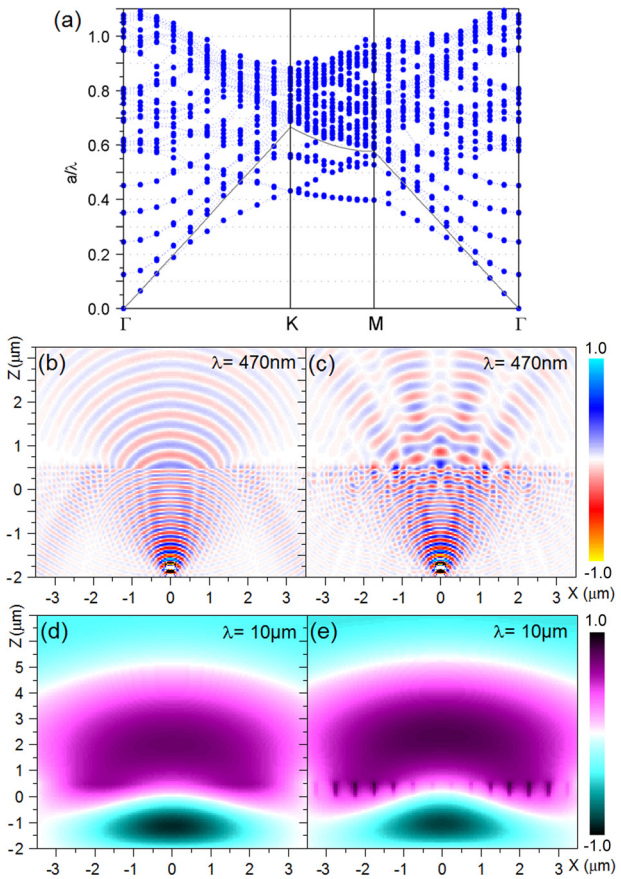

FIG. 3. (a) TE band structure of the PhC computed using the plane wave expansion algorithm. Simulation radiation profiles of continuous-waves at the wavelengths of 470 nm and 10 μm propagating through the flat-top [(b) and (d)] and PhC interfaces [(c) and (e)].

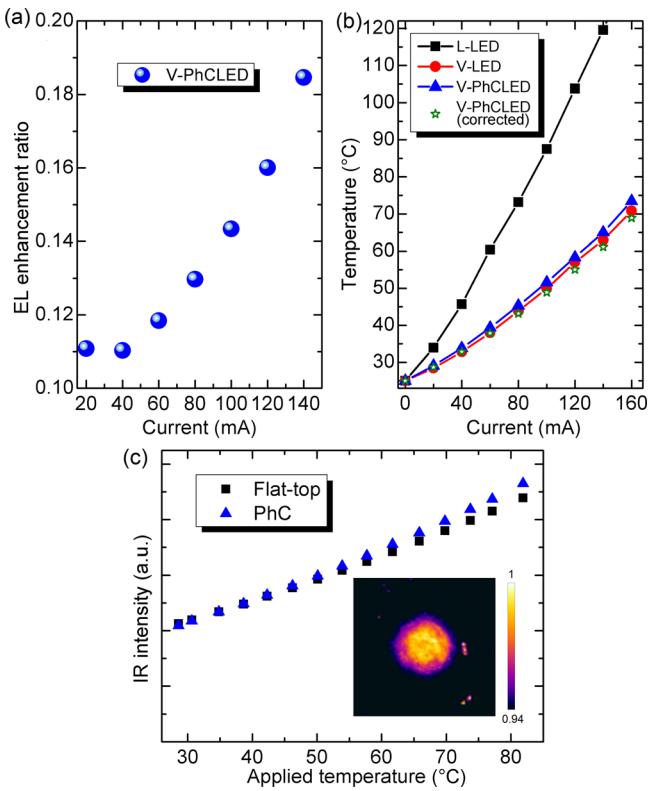

FIG. 4. (a) EL enhancement ratios of the V-PhCLED over the V-LED as calculated from the EL data of Fig. 2. (b) The variations of surface temperatures vs currents as measured by LWIR camera. (c) IR intensities as functions of applied temperatures. The inset shows the LWIR image illustrating intensity contrast between the PhC (circular central region) and the flat-top GaN surface (outside the central region). The scale bar on the right represents the normalized LWIR intensity.

close to the ambient temperature. Hence, the earlier-made assumption of negligible thermal effect experienced by the devices at this low current is justified. Subsequently, the temperatures of the thin-film LEDs rise at much slower rates than the L-LED. At 140 mA, whereby light output saturates, the L-LED attains a surface temperature of 120 °C or 57 °C higher than that of the V-LED of 63 °C, which can simply be attributed to poor thermal conductivity of sapphire, exacerbated by higher dynamic resistance. In terms of optical power, the V-LED emits 51% more light than the L-LED, of which 23% is related to changes in IQE which is temperature dependent. According to the temperature dependence of IQE in InGaN/GaN LEDs, as reported in Ref. 14, a reduction of temperature by 57 °C gives rise to an increase of IQE by ~29% based on linear interpolation of the given data, which is in good agreement with our measured data.

The temperature data in Fig. 4(b) also indicate that the V-PhCLED attains higher temperatures than the V-LED over the entire measurement range, which is in stark contradiction to the information conveyed by the optical data. Since the V-PhCLED emits more light with similar I-V characteristics compared to the V-LED, its chip temperature should also be inferred as being lower. This intriguing observation can be explained by interpreting the LWIR data in terms of LWIR signal strength rather than absolute temperature, which has been evaluated based on the assumption of equal emissivities. Therefore, the LWIR data should be interpreted as increased emission of IR signal from the V-PhCLED over the V-LED, rather than increased temperatures. In other words, the PhC structure on the surface of the V-PhCLED enhances LWIR radiation generated from devices.

To further investigate this phenomenon, an identical PhC structure is selectively patterned at the central region of a $5 \times 5\,mm^2$ n-doped GaN sample, leaving the surrounding area flat-top. The sample is then placed on a hot-plate for a sufficiently long period of time to ensure that the entire body reaches thermal equilibrium. The LWIR intensities are evaluated from the temperature readings using Planck's law. The captured LWIR map of the sample is shown in the inset of Fig. 4(c), which reflects the variation of LWIR intensities detected across the sample. Even though the sample attains thermal equilibrium, the LWIR intensities emitted from the PhC and flat-top regions of the sample differ. Figure 4(c) plots the LWIR intensities at the center of the PhC and at the flat-top region of the sample as a function of applied temperatures. When the applied temperature is close to the ambient temperature, the detected LWIR intensities from both points are nearly the same. With an increase of applied temperature, the PhC region emits more IR radiation than the surrounding flat-top surface, with an enhancement factor of 6.9% at 86 °C. Unfortunately, as indicated by the band structure diagram shown in Fig. 3(a), the band folding effect to guided modes is only valid up to near IR wavelengths of ~1.25 μm and thus may not contribute to light extraction in the mid-IR range (5–30 μm). The relation $\Lambda_{cutoff} \approx \lambda/(n_{eff}+1)$ also indicates that a 2-D PhC with a lattice constant (Λ_{cutoff}) of 500 nm is unlikely to introduce any band folding effects at wavelengths >1.6 μm. Therefore, the enhancement of IR intensity is mainly attributed to an enlarged exposed surface area provided by the nano-pillar PhC for heat exchange with the ambient air, thereby promoting the emission of LWIR radiation. To verify this postulation, a similar FDTD simulation is carried out, this time at LWIR wavelengths of 7.5 to 13 μm. The simulated plots of electric-field intensity distribution for an unpatterned GaN/air interface and the PhC at 10 μm are illustrated in Figs. 3(d) and 3(e), respectively. Quantitatively, the PhC enhances IR radiation by 4.2%–7.4% between 7.5 and 13 μm, consistent with the experimental data obtained from LWIR thermography. Although higher LWIR intensities are detected from the PhC region, the temperatures of PhC and flat-top regions are actually identical. In other words, the emissivity of the PhC region has been enhanced, and is determined to be 0.70 (compared to 0.62 of flat-top GaN). Using the true value of emissivity for the PhC, the corrected temperature of the V-PhCLED is evaluated and re-plotted in Fig. 4(b). Evidently, the V-PhCLEDs have the lowest surface temperatures amongst the devices, consistent with the fact that these devices also emit the most light. Therefore, the PhC enhances light extraction in the visible and in the IR simultaneously, so that devices emit more light whilst radiating more heat at higher currents, a feature that is beneficial to the overall efficiencies of the emitters.

In summary, we have demonstrated PhC thin-film vertical LEDs consisting of HCP nano-pillar arrays patterned by NSL. The nano-pillar array functions as a 2-D PhC to extract visible light via diffraction, thus boosting light output power. The device benefits additionally from enhanced IR extraction due to increased surface areas further reducing chip temperatures to give higher IQEs.

This work was jointly supported by the Theme-based Research Scheme (T22-715/12-N) and a General Research Fund (HKU711212E) of the Research Grant Council of Hong Kong.

[1]W. S. Wong, T. Sands, and N. W. Cheung, Appl. Phys. Lett. **72**, 599 (1998).
[2]X. Guo and E. F. Schuber, Appl. Phys. Lett. **78**, 3337 (2001).
[3]T. Fujii, Y. Gao, R. Sharma, E. L. Hu, S. P. DenBaars, and S. Nakamura, Appl. Phys. Lett. **84**, 855 (2004).
[4]C. C. Kao, H. C. Kuo, H. W. Huang, J. T. Chu, Y. C. Peng, Y. L. Hsieh, C. Y. Luo, S. C. Wang, C. C. Yu, and C. F. Lin, IEEE Photonics Technol. Lett. **17**, 19 (2005).
[5]X. H. Wang, W. Y. Fu, P. T. Lai, and H. W. Choi, Opt. Express **17**, 22311 (2009).
[6]H. W. Choi, M. D. Dawson, P. R. Edwards, and R. W. Martin, Appl. Phys. Lett. **83**, 4483 (2003).
[7]S. X. Jin, J. Li, J. Z. Li, J. Y. Lin, and H. X. Jiang, Appl. Phys. Lett. **76**, 631 (2000).
[8]T. N. Oder, J. Shakya, J. Y. Lin, and H. X. Jiang, Appl. Phys. Lett. **83**, 1231 (2003).
[9]J. J. Wierer, A. David, and M. M. Megens, Nat. Photonics **3**, 163 (2009).
[10]K. H. Li and H. W. Choi, J. Appl. Phys. **109**, 023107 (2011).
[11]S. J. Chua, H. W. Choi, J. Zhang, and P. Li, Phys. Rev. B **64**, 205302 (2001).
[12]C. Wiesmann, K. Bergenek, N. Linder, and U. T. Schwarz, Laser Photonics Rev. **3**, 262 (2009).
[13]J. Shakya, K. Knabe, K. H. Kim, J. Li, J. Y. Lin, and H. X. Jiang, Appl. Phys. Lett. **86**, 091107 (2005).
[14]W. W. Chow, Opt. Express **22**, 1413 (2014).